Serotonin receptor 1A–modulated phosphorylation of glycine receptor α3 controls breathing in mice

Till Manzke,[1,2,3] Marcus Niebert,[1,2] Uwe R. Koch,[1] Alex Caley,[4,5] Steffen Vogelgesang,[2] Swen Hülsmann,[1,2] Evgeni Ponimaskin,[1,2] Ulrike Müller,[6] Trevor G. Smart,[5] Robert J. Harvey,[4] and Diethelm W. Richter[1,2]

[1]Department of Neuro- and Sensory Physiology, University of Göttingen, Göttingen, Germany.
[2]DFG Research Center Molecular Physiology of the Brain (CMPB), Göttingen, Germany. [3]Department of Child and Adolescent Psychiatry, University of Göttingen, Göttingen, Germany. [4]Department of Pharmacology, School of Pharmacy, London, United Kingdom.
[5]Department of Neuroscience, Physiology, and Pharmacology, University College London, London, United Kingdom.
[6]Institute for Pharmacy and Molecular Biotechnology (IPMB), University of Heidelberg, Germany.

Rhythmic breathing movements originate from a dispersed neuronal network in the medulla and pons. Here, we demonstrate that rhythmic activity of this respiratory network is affected by the phosphorylation status of the inhibitory glycine receptor α3 subtype (GlyRα3), which controls glutamatergic and glycinergic neuronal discharges, subject to serotonergic modulation. Serotonin receptor type 1A–specific (5-HTR$_{1A}$–specific) modulation directly induced dephosphorylation of GlyRα3 receptors, which augmented inhibitory glycine-activated chloride currents in HEK293 cells coexpressing 5-HTR$_{1A}$ and GlyRα3. The 5-HTR$_{1A}$–GlyRα3 signaling pathway was distinct from opioid receptor signaling and efficiently counteracted opioid-induced depression of breathing and consequential apnea in mice. Paradoxically, this rescue of breathing originated from enhanced glycinergic synaptic inhibition of glutamatergic and glycinergic neurons and caused disinhibition of their target neurons. Together, these effects changed respiratory phase alternations and ensured rhythmic breathing in vivo. GlyRα3-deficient mice had an irregular respiratory rhythm under baseline conditions, and systemic 5-HTR$_{1A}$ activation failed to remedy opioid-induced respiratory depression in these mice. Delineation of this 5-HTR$_{1A}$–GlyRα3 signaling pathway offers a mechanistic basis for pharmacological treatment of opioid-induced apnea and other breathing disturbances caused by disorders of inhibitory synaptic transmission, such as hyperekplexia, hypoxia/ischemia, and brainstem infarction.

Introduction

The motor control of regular rhythmic breathing of mammals originates from a neuronal network in the lower brainstem that includes the bilateral ventral groups of respiratory neurons (VRG) with the pre–Bötzinger complex (pre-BötC; refs. 1, 2) and receives important feedback control through postinspiratory neurons of the pontine respiratory group (PRG; refs. 3, 4). This distributed respiratory network contains various types of respiratory neurons (5) capable of generating alternating burst discharges that are necessary for rhythmic breathing movements. Under normal in vivo conditions, rhythm generation depends on coordinated integration of excitatory and inhibitory synaptic inputs to the neurons that determines membrane potential fluctuations and periodic adjustment of voltage-gated currents involved in neuronal bursting (6–8). Inhibitory synaptic interactions are vital, as they both impose the voltage changes required for initiation of endogenous respiratory bursting and control the burst pattern. Another indispensable function of these interactions is to terminate respiratory bursts during transitions among the distinct phases of the respiratory cycle that are determined by activity of antagonistic neurons (8–10). This critical process of burst termination is largely controlled by glycine receptors (GlyRs), since dysfunction or deletion of inhibitory glycinergic

transmission abolishes regular breathing (11–13). This clinically significant consequences, such as prolonged breath-holding episodes (also called inspiratory apnea or apneusis; refs. 14–16), leading to deleterious hypoxic conditions as seen in genetic diseases, such as Rett syndrome (17) or hyperekplexia (commonly known as startle disease; ref. 13). Similar breathing difficulties can also occur following ischemia and stroke (18, 19) and as a result of deep anesthesia (20), opiate abuse (21), head trauma, degenerative brain diseases (15), and alcoholism (22).

Treatments involving pharmacological manipulations of intracellular signaling pathways, particularly those involving the serotonin receptor (5-HTR) family, have been considered in the past (23), but their intracellular basis have not been fully established. These and other GPCRs (24) are abundantly expressed in the VRG and pre-BötC (21, 25). Many of their signaling pathways converge on adenylyl cyclase (AC), which regulates intracellular cAMP levels and, consequently, the activity of cAMP-dependent PKA. Accordingly, it is of both clinical and basic importance to unravel the different processes that determine the dynamic adjustments within neuronal networks associated with rhythmic breathing through the regulation of intracellular cAMP levels in vivo (14–16, 23, 25). One specific question concerns the convergence and separation of agonistic and antagonistic GPCR signaling within respiratory cells. The hypothesis tested in this study was that intracellular signaling occurs in a receptor-specific pattern along parallel intracellular pathways. Specifically,
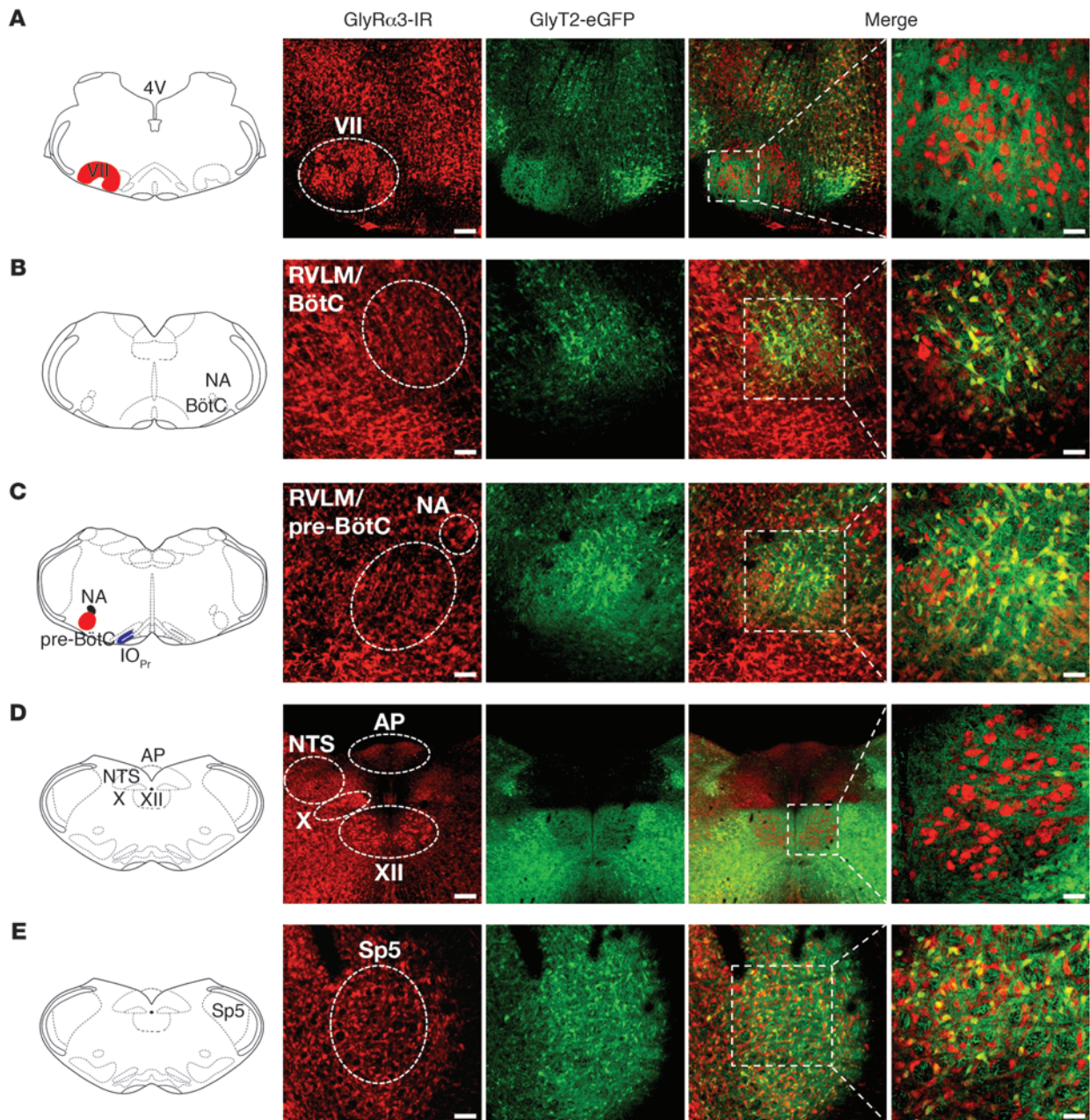
Figure 1
Expression of GlyRα3 in the brainstem. GlyRα3 immunoreactivity (GlyRα3-IR) showed almost-ubiquitous expression in the brainstem. Although there was no coexpression of GlyRα3 in motor nuclei like the facial nucleus (VII; **A**) and hypoglossal nucleus (XII; **D**) with GlyT2-eGFP neurons, GlyRα3 was expressed on glycinergic neurons within the BötC (**B**), pre-BötC (**C**), and spinal trigeminal nucleus (Sp5; **E**). Higher-magnification views of the merged images are shown at right. Scale bars: 200 μm (**A** and **D**); 100 μm (**B**, **C**, and **E**); 50 μm (higher magnification). AP, area postrema; IO$_{Pr}$, principal nucleus of the inferior olive; NA, nucleus ambiguus; NTS, nucleus of the solitary tract; RVLM, rostral ventrolateral medulla.

we investigated the molecular mechanisms of the interaction between glycinergic and 5-HTR control of rhythmic breathing (23, 25). Our findings demonstrate that an interaction between serotonin receptor type 1A (5-HTR$_{1A}$) and inhibitory glycine receptor α3 subtype (GlyRα3) stabilized breathing and counteracted its μ-opioid receptor–induced (μOR-induced) depression. These findings may lead to novel therapeutic interventions to treat breathing disorders.

Results
Receptor profiling in excitatory and inhibitory respiratory neurons. Glycinergic inhibition of antagonistic neurons is a fundamental process in respiratory network operation that enables stable rhythmic breathing. It is necessary to regulate steady augmentation of inspiratory activity required for continuous inhalation and afterward terminate inspiratory activity to allow its slow decline during postinspiration, as seen in efferent phrenic nerve (PN) output (10).
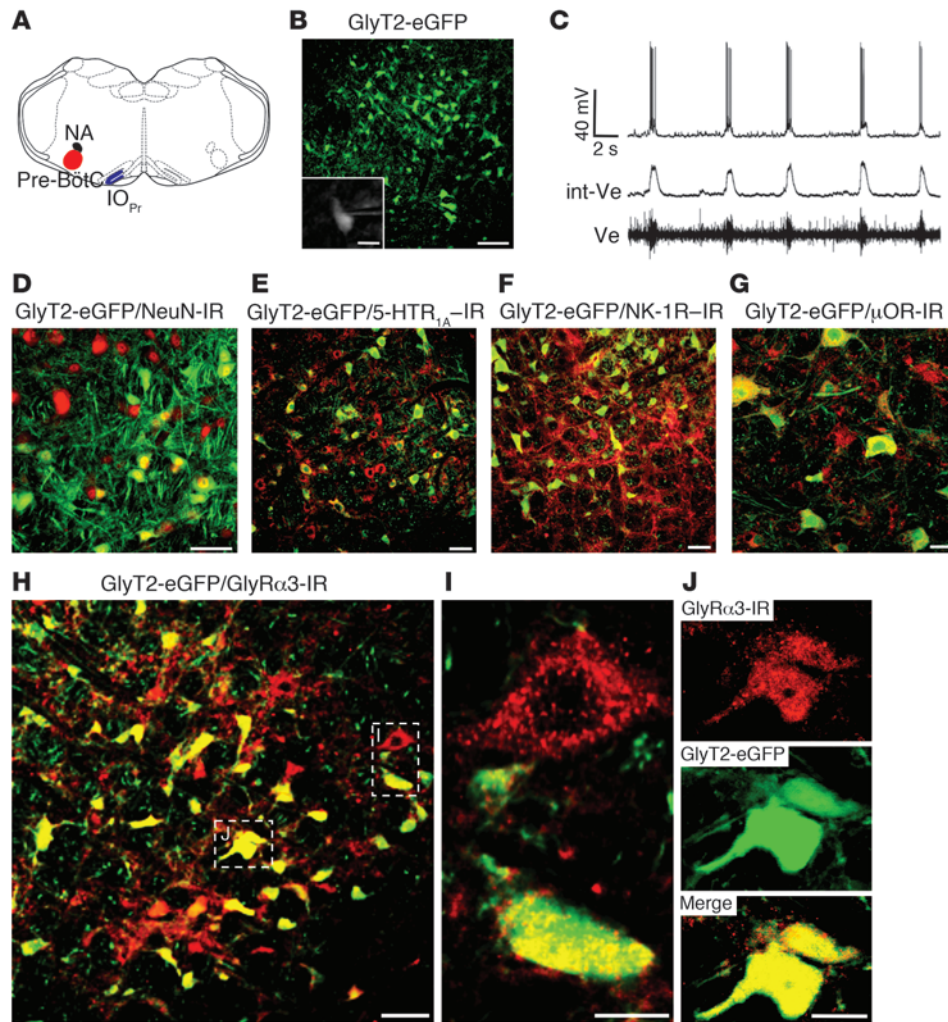
Figure 2
Receptor profiling of glycinergic inhibitory pre-BötC neurons. (**A**) Schematic representation of the pre-BötC with its anatomical landmarks. (**B**) Expression of eGFP under control of the neuronal GlyT2 promoter demarcates inhibitory glycinergic neurons (green) within the pre-BötC. (**C**) Respiratory activity of glycinergic neurons (see **B**, inset) was identified by correlation of rhythmic depolarizations of the membrane potential (top trace) with the changes of extracellular field potentials (Ve) recorded from the pre-BötC shown in integrated and original form. (**D**) Expression of the neuron-specific nuclear protein NeuN (Cy5; red). NeuN immunoreactivity was performed to determine the amount of inhibitory GlyT2-eGFP–expressing neurons in the pre-BötC. (**E**) GlyT2-eGFP–positive neurons expressed abundant 5-HTR$_{1A}$ (Cy5; red) in the pre-BötC. (**F**) About 18% of GlyT2-eGFP–positive neurons were immunostained for NK-1R (Cy5; red), a known marker of respiratory neurons. This corresponds with the approximately 20% of neurons that revealed ongoing inspiratory discharges, as verified in visually controlled whole-cell recording with microelectrodes (see **B** and **C**). (**G**) Expression of μORs on GlyT2-eGFP–positive neurons. (**H–J**) Positive immunolabeling of GlyRα3 included not only GlyT2-eGFP–negative cells (**I**), but also GlyT2-eGFP–positive neurons (green), as illustrated by individual cell staining (**J**). Boxed regions in **H** are shown at higher magnification in **I** and **J**, as indicated. Scale bars: 100 μm (**B**); 20 μm (**B**, inset, and **G**); 50 μm (**D–F** and **H**); 10 μm (**I** and **J**).

in the whole brainstem (Figure 1). In general, GlyRα3 was found in GlyT2-negative cells, but unexpectedly, in the BötC and pre-BötC, which is essential for respiratory rhythm generation (1, 2), GlyRα3 was also expressed in GlyT2-positive cells (Figure 1, B and C). We focused our immunohistochemical study on the entire 200-μm extension of the bilateral pre-BötC (5 consecutive 40-μm transverse sections; n = 3 mice), which revealed that glycinergic neurons represented 55.50% ± 1.56% of total neurons (58.07 ± 3.07 GlyT2-eGFP cells of 103.70 ± 2.82 NeuN-immunoreactive cells/section), as identified by labeling with the vertebrate neuron-specific nuclear protein neuronal nuclei (NeuN; Figure 2D). A large number of the GlyT2-eGFP–positive cell population also expressed the neurokinin-1 receptor (NK-1R), which is characteristic for respiratory neurons (27, 28). GlyT2-eGFP–positive neurons represented 18.21% ± 0.79% (20.80 ± 1.35 NK-immunoreactive cells of 113.00 ± 3.11 GlyT2-eGFP cells/section) of NK-1R–positive cells that were intermingled with NK-1R–positive, but GlyT2-eGFP–negative, neurons (Figure 2F). Whole-cell recordings in the in vitro brainstem slice preparation confirmed that greater than 20% of these GlyT2-eGFP–labeled glycinergic inhibitory neurons exhibited ongoing inspiratory discharges (Figure 2, B and C, and ref. 29).

Another key finding was prominent GlyRα3 immunoreactivity (30) in pre-BötC neurons (Figure 2H), including NK-1R–positive excitatory respiratory neurons and GlyT2-eGFP–labeled inhibitory neurons. The numerous GlyRα3 puncta present on the surface of inhibitory glycinergic neurons (Figure 2, I and J) indicated that GlyT2-positive cells themselves receive inhibitory glycinergic

This important function correlates with the large number of glycinergic VRG and pre-BötC neurons that are characterized by the expression of the neuronal glycine transporter 2 (GlyT2). We used transgenic mice expressing enhanced GFP (eGFP) under the control of the GlyT2 promoter (GlyT2-eGFP; ref. 26) to study receptor expression on glycinergic neurons. First, we analyzed the expression of GlyRα3 and found it to be almost ubiquitously expressed

inputs. Our inference is that not only excitatory, but also inhibitory, neurons receive afferent glycinergic inputs, which hence must disinhibit neurons they innervate. This makes the rhythm-generating pre-BötC (1) an important target for modulating adjustment of breathing movements in vivo. However, by taking a systems overview, such modulation must involve not only preinspiratory or early-inspiratory neurons in pre-BötC (28), but also glycinergic
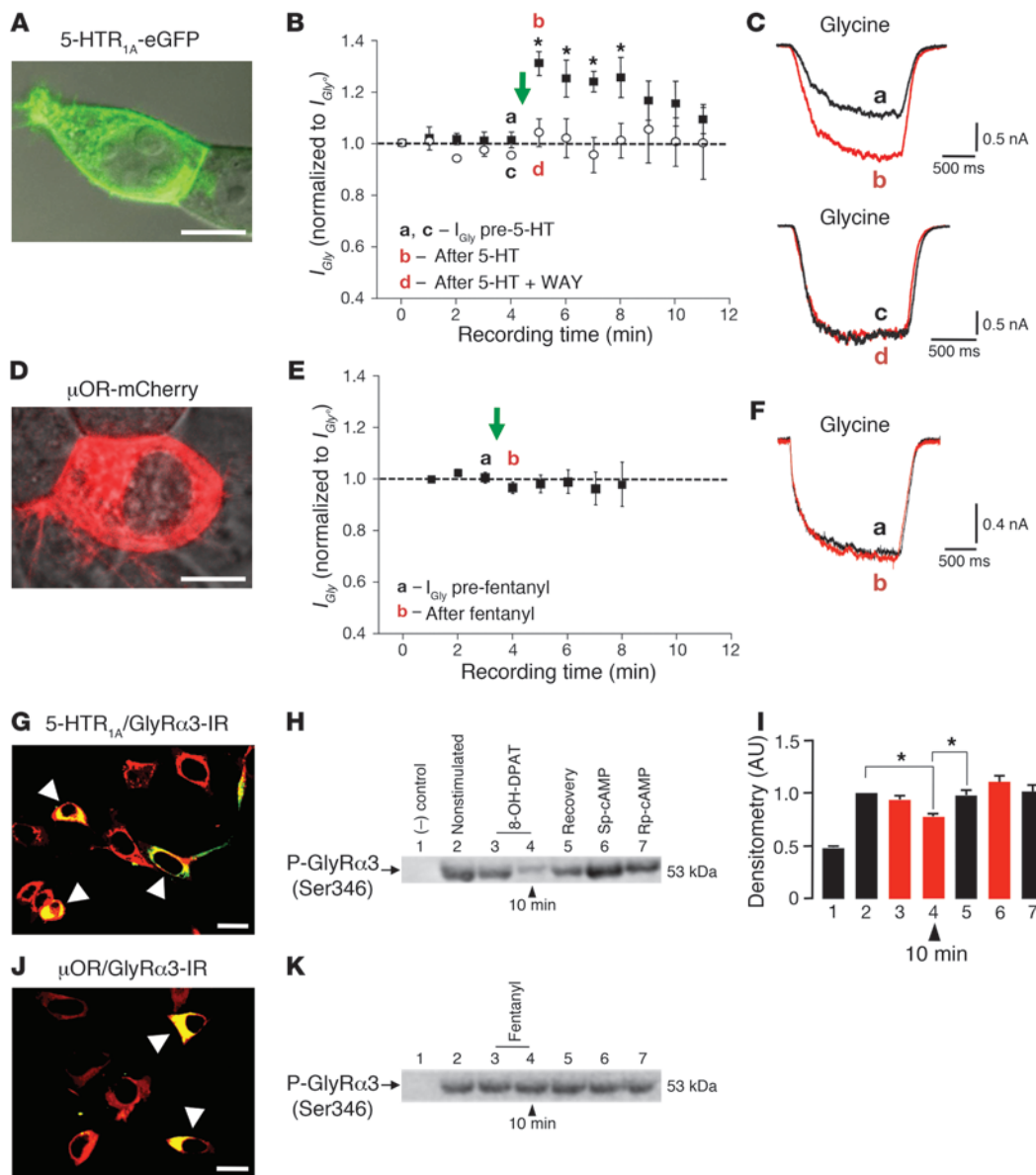
Figure 3
Altered modulation of the respiratory network in *Glra3⁻/⁻* mice and 5-HTR₁ₐ–induced augmentation of GlyRα3 function via PKA in recombinant systems. (**A**) HEK293 cell expressing 5-HTR₁ₐ–eGFP. (**B**) Time stability profile for I_{Gly} recorded from cells coexpressing GlyRα3L and 5-HTR₁ₐ. Currents were activated by rapid application of glycine (EC₂₀) before and after activation of 5-HTR₁ₐ by 5-HT (green arrow), with (white circles) or without (black squares) coapplication of the selective 5-HTR₁ₐ inhibitor WAY 100635. All currents were normalized to I_{Gly} at 0 minutes ($I_{Gly}°$). Time points at which the currents in **C** were taken are denoted. (**C**) Individual I_{Gly} activated by glycine, before and after 5-HTR₁ₐ activation and before and after coapplication of 5-HT and WAY 100635. (**D**) HEK293 cell expressing μOR-mCherry. (**E** and **F**) Time stability profiles for I_{Gly} from cells coexpressing GlyRα3L and μOR, analogous to **B** and **C**. (**G** and **H**) HEK293 cells expressing 5-HTR₁ₐ and GlyRα3 (**G**) and immunoblot detection (**H**) of the phosphorylation status of GlyRα3 before and after drug application. Lane 1, negative control; lane 2, before drug application; lanes 3 and 4, GlyRα3 phosphorylation (decreased after selective activation of 5-HTR₁ₐ); lane 5, recovery of phosphorylation after 45 minutes. Activation of PKA with Sp-cAMP, a potent and specific activator of cAMP-dependent protein kinases, increased phosphorylation (lane 6), while Rp-cAMP, a cAMP analog and competitive inhibitor of cAMP-dependent protein kinase I and II, decreased phosphorylation (lane 7). (**I**) Statistics after densitometric measurement ($n = 4$). *$P < 0.05$. (**J** and **K**) HEK293 cells expressing μOR and GlyRα3 (**J**) and immunoblot analogous to **H** (**K**). Scale bars: 5 μm (**A** and **D**); 20 μm (**G** and **J**).

postinspiratory neurons, which are localized in the rostral VRG and also in the pons (3, 4).

Serotonergic innervation of inhibitory glycinergic neurons. Since synaptic inhibition is modulated by serotonin (5-HT; ref. 21), we examined

the expression profiles of 5-HTR₁ₐ and μORs in inhibitory glycinergic neurons. To verify 5-HTR₁ₐ expression on glycinergic neurons within the bilateral pre-BötC, we analyzed in total 2,860 GlyT2-eGFP positive cells (5 consecutive 40-μm transverse sections; $n = 5$

mice). The majority of these glycinergic neurons, 86.25% ± 1.11% (98.60 ± 1.97 cells expressing 5-HTR$_{1A}$ of 114.40 ± 1.96 GlyT2-eGFP cells/section; n = 5), revealed strong 5-HTR$_{1A}$ immunoreactivity (Figure 2E). To also verify μOR expression in these glycinergic neurons, we analyzed in total 1,423 GlyT2-eGFP neurons and observed that a majority 90.94% ± 1.06% (86.27 ± 1.66 μOR-immunoreactive cells of 94.87 ± 1.51 GlyT2-eGFP cells/section; n = 3) also expressed μOR (Figure 2G). In conclusion, all types of pre-BötC neurons seemed to be subject to G$_{i/o}$-controlled (e.g., via 5-HTR$_{1A}$ and μOR) AC-cAMP-PKA signaling pathways.

Serotonergic modulation of GlyRα3. The continuous release of serotonin from afferent terminals of spontaneously active Raphé nuclei (31, 32) and the strong expression of GlyRα3 in both excitatory and inhibitory pre-BötC neurons suggested the possibility of in vivo modulation of glycinergic inhibition via changes in PKA-mediated GlyR phosphorylation. The likely target is serine 346 within the GlyRα3 M3–M4 loop, which forms part of a strong PKA consensus sequence (RESR; refs. 30, 33). To demonstrate that GlyRα3 is capable of forming the molecular target for 5-HT, we coexpressed eGFP-tagged 5-HTR$_{1A}$ and GlyRα3 in HEK293 cells (Figure 3, A and G). Activation of 5-HTR$_{1A}$ with 1 μM serotonin enhanced Cl$^-$ currents activated by 100 μM glycine (referred to herein as glycine-activated Cl$^-$ currents [I_{Gly}]; equivalent to the EC$_{20}$) by up to 30% (Figure 3, B and C; n = 6/8 cells). The effect was specifically inhibited by application of the selective 5-HTR$_{1A}$ antagonist WAY 100635 (2 μM; n = 4; Figure 3, B and C). This suggests that activation of 5-HTR$_{1A}$ coupled to G$_{i/o}$ inhibits PKA, inducing steady dephosphorylation of GlyRα3 and thus potentiating I_{Gly}. Indeed, Western blotting with a phosphospecific monoclonal antibody that selectively recognizes GlyRα3 phospho–serine 346 (see Methods) revealed that activation of 5-HTR$_{1A}$ by 8-hydroxy-2-(di-N-propylamino)-tetralin hydrobromide (8-OH-DPAT; 50 μM) induced GlyRα3 dephosphorylation by greater than 20% (decline from 1.00 AU unstimulated control to 0.7726 ± 0.0245 AU 10 minutes after 5-HTR$_{1A}$; P < 0.05; n = 4; Figure 3, H and I). Importantly, in similar heterologous expression studies, we also demonstrated that selective μOR stimulation with 30 nM fentanyl did not change GlyRα3 phosphorylation in HEK293 cells coexpressing GlyRα3 and μOR (Figure 3, J and K). This lack of effect following μOR activation was also evident from monitoring the time stability of I_{Gly} after application of 30 nM fentanyl to HEK293 cells coexpressing μOR and GlyRα3 (n = 6; Figure 3, D–F). Thus, under normal conditions, GlyRα3 is selectively modulated by 5-HTR$_{1A}$, but not by μOR activation.

Characterization of the GlyRα3 knockout mouse. In the VRG, GlyRα3-deficient mature mice (*Glra3*$^{-/-}$; age P30, n = 3) expressed the genes for GlyRα1 (*Glra1*) and also weakly GlyRα2 (*Glra2*), but lacked GlyRα4 (*Glra4*), as did WT mice (age P30; n = 3), while GlyRβ (*Glrb*) and gephyrin (*Gphn*) were maintained (Figure 4D). The mRNA level for GlyT2 (*Slc6a5*) was slightly reduced, but that for glycine transporter 1 (*Slc6a9*) was unchanged.

Functional testing of the network response to 5-HTR$_{1A}$ modulation of GlyRα3 was performed using the in situ perfused mouse brainstem–spinal cord preparation, which preserves the complete respiratory network and generates a normal activity pattern (34) different from in vitro preparations (2). PN output activity showed an irregular respiratory rhythm (Figure 4, E–H). In *Glra3*$^{-/-}$ mice, the most stable phase activity was seen in the inspiratory bursts. Their phase duration was not affected (WT, 0.3177 ± 0.0078 s; *Glra3*$^{-/-}$, 0.2968 ± 0.0079 s; P = NS), showing coefficients of varia-

tion (CV) that were comparable (WT, 16.26% ± 0.90%; *Glra3*$^{-/-}$, 17.14% ± 1.10%; n = 5). The expiratory phase duration was slightly prolonged (WT, 2.839 ± 0.117 s; *Glra3*$^{-/-}$, 3.874 ± 0.576 s; P = NS); however, the postinspiratory phase duration varied greatly (WT, 0.082 ± 0.007 s; *Glra3*$^{-/-}$, 0.442 ± 0.065 s; P < 0.001), revealing a CV increase from 18.01% ± 5.16% in WT to 67.85% ± 30.82% in *Glra3*$^{-/-}$ mice.

Systemic modulation of specific receptors and compound network reaction. Because GlyRα3 appears to be an important GlyR subtype in the pre-BötC and adjacent VRG, glycinergic inhibition should be potentiated by 5-HTR$_{1A}$ activation, which inhibits AC and thus reduces PKA activity. In the in vivo–like preparation, we applied drugs systemically via intraarterial infusion (10–20 μl/min flow rate), while the output of the respiratory network was measured by PN recordings. Moving averages of PN burst discharges measured together with burst frequencies allowed an estimate of relative PN minute activity (mPNA; Figure 5), corresponding to the physiological respiratory minute volume before and after stimulation and/or following selective inhibition of specific receptors. After application of the 5-HTR$_{1A}$ agonist 8-OH-DPAT (10 μM), relative mPNA was augmented 28% (from control 1.00 ± 0.08 AU to 1.28 ± 0.13 AU; P < 0.05; n = 5), as evidenced by enhanced burst frequency (from control 21.70 ± 1.79 bursts/min to 27.70 ± 2.73 bursts/min; P < 0.05; Figure 5A). This finding was similar to the 5-HTR$_{1A}$–mediated reinforcement of glycinergic inhibition. A remarkable observation was that the stimulatory effects of 10 μM 8-OH-DPAT were entirely blocked by application of 2 μM of the GlyR antagonist strychnine. Strychnine application alone provoked a significant increase of relative mPNA (from 1.00 ± 0.21 AU to 1.82 ± 0.19 AU, P < 0.05; n = 5), but remained unaltered after additional activation of 5-HTR$_{1A}$ with 8-OH-DPAT (1.87 ± 0.15 AU, P = NS; data not shown).

Absence of respiratory network modulation in Glra3$^{-/-}$ *mice.* As anticipated, selective stimulation of 5-HTR$_{1A}$ by 10 μM 8-OH-DPAT in *Glra3*$^{-/-}$ mice failed to augment relative mPNA (0.99 ± 0.07 AU versus control 1.00 ± 0.06 AU, P = NS) and burst frequency (18.40 ± 1.16 bursts/min vs. 18.20 ± 1.25 bursts/min, P = NS; n = 5; Figure 5B). This indicates that GlyRα3 is the only significant molecular target for 5-HTR$_{1A}$–mediated modulation of PKA with regard to the control of breathing. Although GlyRα1 protein was still expressed in the *Glra3*$^{-/-}$ mouse (Figure 4C), it is not subject to modulation by PKA (30). Following the notion that regular breathing critically depends on adaptable glycinergic inhibition (8–10), and to demonstrate that this modulation is clinically relevant, we tested whether 5-HTR$_{1A}$–induced reinforcement of inhibitory postsynaptic glycinergic currents could compensate for a general opioid-produced depression of neuronal excitability in the network (35). Systemic activation of 5-HTR$_{1A}$ in WT mice was indeed effective in averting opioid-induced respiratory apnea. The relative mPNA was strongly decreased after application of 18.9 nM fentanyl (decline from control 1.00 ± 0.10 AU to 0.04 ± 0.03 AU, P < 0.01; n = 5), but recovered after 5-HTR$_{1A}$ activation with 10 μM 8-OH-DPAT to 0.94 ± 0.05 AU (P < 0.01). The burst frequency changed from control levels of to 1.00 ± 0.76 bursts/min to 23.00 ± 2.33 bursts/min (P < 0.01) after fentanyl application and recovered to 21.70 ± 1.12 bursts/min after administration of 8-OH-DPAT (P < 0.01; n = 5; Figure 5C). This is in accordance with previous studies on other rodent models (21, 25, 36, 37). The effect was blocked in *Glra3*$^{-/-}$ mice and replaced by an additional depression of rhythmic discharges (relative mPNA, from control 1.00 ± 0.05 AU to 0.07 ± 0.05 AU after 18.9 nM fentanyl, P < 0.01; with persistent depression to 0.05 ± 0.04 AU after 10 μM
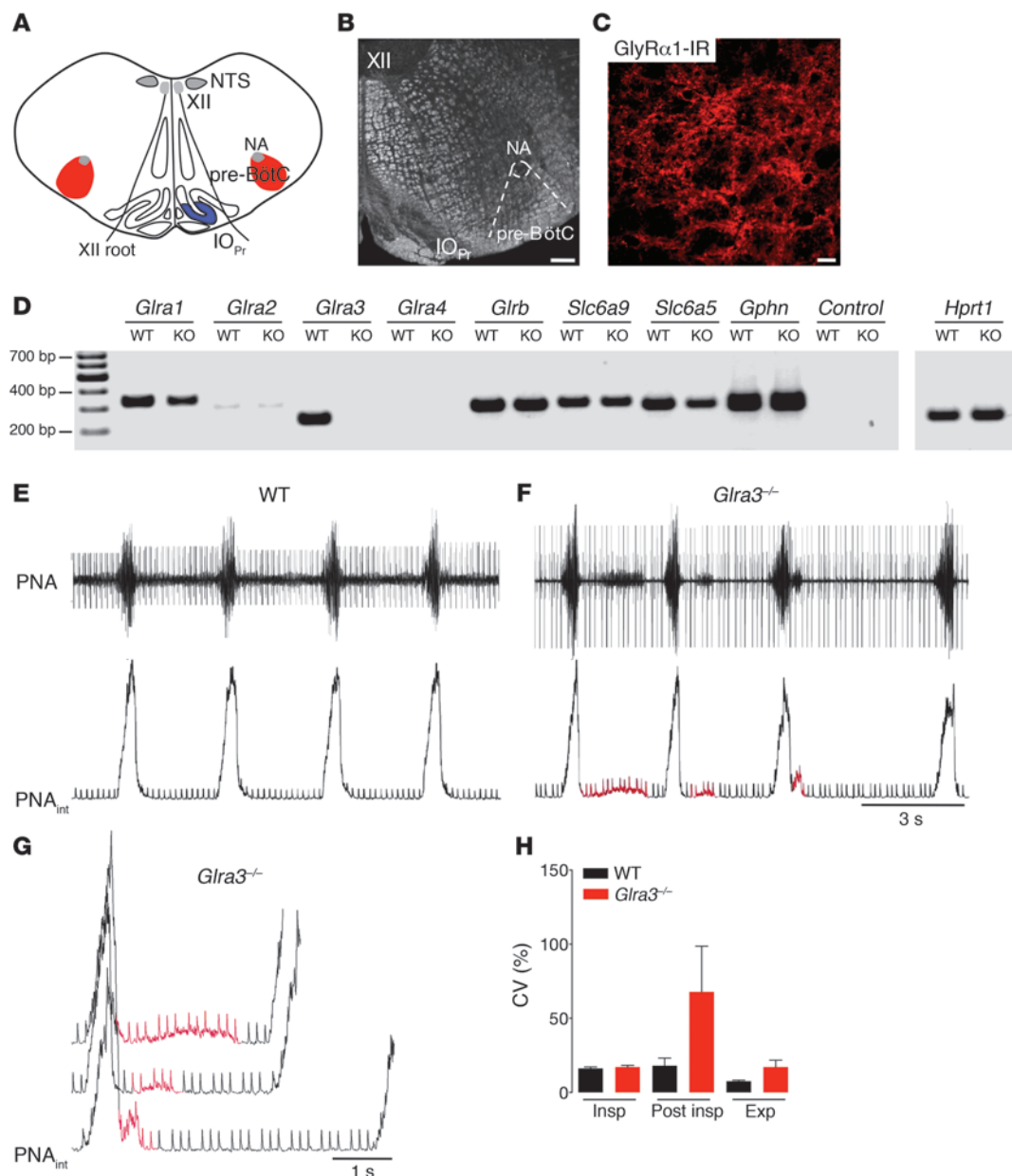
Figure 4
Characterization of the respiratory phenotype of *Glra3⁻/⁻* mice. (**A**) Schematic of the pre-BötC with its anatomical landmarks. (**B**) Overview of **C**, which shows dense GlyRα1 immunoreactivity in the pre-BötC of *Glra3⁻/⁻* mice. Scale bars: 200 μm (**B**); 20 μm (**C**). (**D**) RT-PCR analysis of pre-BötC tissue of WT and *Glra3⁻/⁻* mice revealed expression of known components of glycinergic synapses. In WT mice, the receptor transcripts of GlyRα3 and GlyRα1 were the 2 most abundant in the pre-BötC. (**E**) Respiratory pattern of the WT mouse represented by the PNA in original and integrated (PNA$_{int}$) forms. (**F**) In contrast to WT mice, *Glra3⁻/⁻* mice showed high variability in the post-inspiratory phase. (**G**) Post-inspiratory disturbances (red) of *Glra3⁻/⁻* at higher magnification, with superposition of 3 bursts derived from **F**. (**H**) CV (± SEM) of the duration of each phase of the respiratory cycle (inspiration, post-inspiration, and expiration) of WT versus *Glra3⁻/⁻* mice.

8-OH-DPAT, P = NS; n = 5; Figure 5D). Taken together, our results demonstrate that pharmacotherapy with 5-HTR$_{1A}$ agonists induces specific augmentation of glycinergic currents via GlyRα3 and thereby protects against opioid-induced apnea.

Discussion

In vivo, respiratory activity is generated by the pre-BötC, which communicates with the adjacent VRG and also with respiratory neurons in the pons (1, 3, 4). In all mammalian species tested, normal rhythm generation depended on reciprocal inhibitory interactions between antagonistic groups of neurons, wherein glycinergic interneurons control respiratory phase transitions during pre- and postinspiration (refs. 10, 13, 38, 39, and Supplemental Figure 1; supplemental material available online with this article; doi:10.1172/JCI43029DS1). Such synaptic feedback from distributed neuronal activities must be integrated in the rhythm-generat-
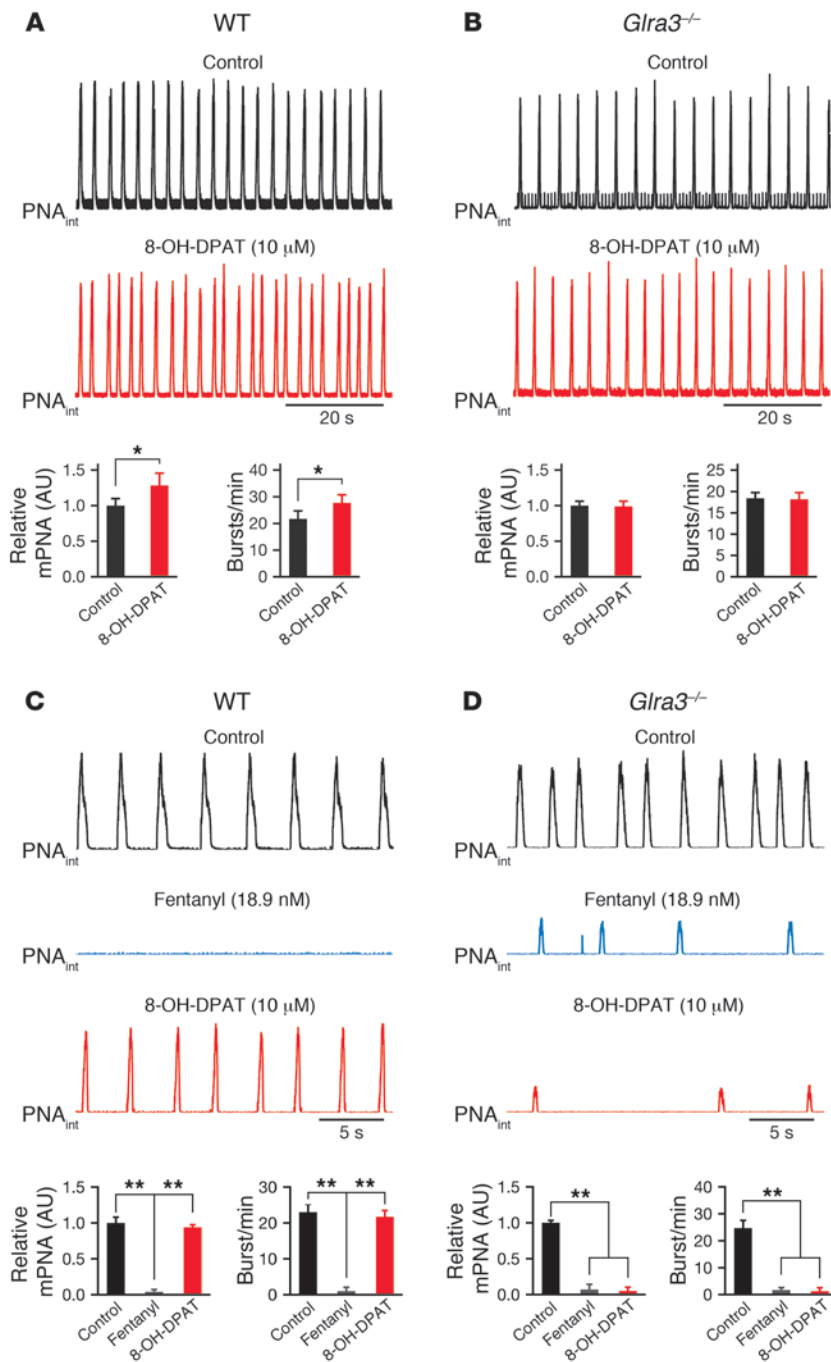
Figure 5
Altered modulation of the respiratory network in *Glra3−/−* mice. (**A** and **B**) Activation of 5-HTR$_{1A}$ using 8-OH-DPAT increased respiratory activity in WT mice (**A**), whereas *Glra3−/−* mice did not show a significant change of mPNA (**B**). Black traces represent integrated mPNA under control conditions. (**C**) Systemic administration of fentanyl significantly reduced or blocked mPNA in WT mice. Respiratory activity was recovered to control levels after stimulation of 5-HTR$_{1A}$ with 8-OH-DPAT. (**D**) *Glra3−/−* mice responded to fentanyl-induced μOR stimulation with an additional decline of spontaneous rhythmic discharges and reinforcement of respiratory depression that could not be recovered by 5-HTR$_{1A}$ stimulation with 8-OH-DPAT. Data are mean ± SEM. *$P < 0.05$; **$P < 0.01$.

phorylation of GlyRα3, thereby potentiating I_{Gly}. Interestingly, previous studies have demonstrated that 5-HTR$_{1A}$ signal transduction proceeds via inhibitory Giα3 proteins (43), while μOR signaling is mediated through Giα2 (44, 45), which suggests that both pathways operate independently. Consistent with these findings, we found that enhancement of glycinergic inhibition via GlyRα3 was controlled by 5-HTR$_{1A}$, while it was unaffected by μOR stimulation (Figure 3 and Supplemental Figure 2).

Although 5-HTR$_{1A}$ signaling specifically targeted GlyRα3 at the cellular level, systemic application of 5-HTR$_{1A}$ agonists must exert both direct and indirect effects within the entire network. The pre-BötC is a clear target for serotonergic neuromodulation and possesses all the necessary molecular components, but neighboring regions of the VRG and even the PRG may also be involved. The activation of 5-HTR$_{1A}$ potentiated glycinergic currents in all postsynaptic neurons receiving glycinergic inputs, including inhibitory glycinergic neurons themselves (Figure 2). The 5-HTR$_{1A}$–induced potentiation of postsynaptic GlyRα3 inhibition of glycinergic neurons will depress their output discharges and cause disinhibition in the postsynaptic neurons they innervate (10, 15). This is consistent with

ing pre-BötC (1, 28). It is therefore not surprising that greater than 50% of neurons within the pre-BötC are glycinergic, as evidenced by strong expression of GlyT2 (21, 40). Furthermore, rhythmic respiratory activity is disturbed when glycinergic synapses dysfunction as a result of genetic lesions (13, 41) or when GlyRs are blocked by strychnine (11, 12).

The present study revealed that both excitatory and inhibitory respiratory neurons of the pre-BötC and adjacent VRG abundantly expressed GlyRα3, a key target for modulation by PKA (30) that operates under the permanent control of a variable 5-HT release from Raphé neurons (32, 42). Selective activation of G$_{i/o}$-coupled 5-HTR$_{1A}$ inhibited PKA, which consequently led to reduced phos-

a previous report (21) demonstrating that systemic 5-HTR$_{1A}$ stimulation induces powerful depression of the discharge of inhibitory early-inspiratory neurons. This releases antagonistic postinspiratory neurons from synaptic inhibition, allowing them to fire during the inspiratory phase, which ultimately terminates inspiration and consequently increases burst frequency. Importantly, however, respiratory rhythmicity is maintained, because periodic inhibition is potentiated and its membrane hyperpolarization establishes the biophysical condition for endogenous burst generation (46, 47).

Using our multidisciplinary approach, we have demonstrated that synaptic GlyRs are the critical target for 5-HTR$_{1A}$ modulation of respiratory network functions. The 5-HTR$_{1A}$–induced reinforce-

ment of synaptic inhibition is an attractive target for therapeutic interventions aimed at counteracting various forms of arrhythmic breathing. Taking just one aspect, we demonstrated that potentiation of GlyRα3 function by 5-HTR$_{1A}$ activation was capable of recovering opioid-induced apnea in WT mice, an effect that was ablated in $Glra3^{-/-}$ mice. We envisage that the delineation of the 5-HTR$_{1A}$–GlyRα3 signaling pathway will have several applications in translational medicine, for example, in the controlled pharmacological revival of spontaneous breathing after deep opiate narcosis in anesthesia. Similarly, by activating this pathway, we may be able to protect against life-threatening opiate overdose or poisoning with analgesics. Our findings could even lead to novel treatment strategies for inflammatory pain (30), since 5-HTR$_{1A}$ activation could oppose prostaglandin E2 receptor–mediated PKA phosphorylation of GlyRα3. Finally, given that $Glra3^{-/-}$ mice showed irregular respiratory rhythm under normal conditions, we would advocate that the *GLRA3* gene be considered as a strong candidate for genetic screening in human disorders of rhythmic breathing.

Methods

Experimental procedures were performed in accordance with European Community and NIH guidelines for the care and use of laboratory animals. This study was approved by the Ethics Committee of Georg-August University (Göttingen, Germany).

Perfused brainstem–spinal cord preparation

Experiments on the in vivo–like in situ brainstem spinal cord preparation were performed on C57BL6 mice (P20–P25) or $Glra3^{-/-}$ mice (P30). $Glra3^{-/-}$ mice were generated by deleting exon 7 of $Glra3$ (encoding the pore-lining M2 transmembrane domain) using the Cre-LoxP gene targeting system. This targeted deletion is known to result in a loss of functional GlyRα3 in spinal cord (30) and retina (48). For isolating the in situ brainstem–spinal cord from higher brain areas, animals were deeply anesthetized with halothane until apnea occurred and they were unresponsive to a forepaw pinch. Animals were then decerebrated at the precollicular level, cerebellectomized, and bisected below the diaphragm, and their skin was removed. The upper body was placed in a recording chamber and perfused retrogradely at 10–20 ml/min via the thoracic aorta with ACSF (1.25 mM MgSO$_4$; 1.25 mM KH$_2$PO$_4$; 5 mM KCl; 125 mM NaCl; 2.5 mM CaCl$_2$; 25 mM NaHCO$_3$; 10 mM glucose; 0.1785 mM Ficoll 70) and aerated with carbogen (5% CO$_2$, 95% O$_2$; pH 7.35). The perfusate was warmed to 30°C (as measured in the skull base), filtered twice, and recirculated. Vecuronium bromide (3.9 μM) was added for muscle relaxation. The perfusion pressure was set to 50–65 mmHg. Using a glass suction electrode, PN discharges were recorded as an index of central respiratory rhythm. Drugs were added to the perfusate for specific pharmacological manipulation of serotonin, μOR, or GlyRs.

Rhythmic slice preparation

Transverse 200-μm slices were cut from the caudal medulla at the level of the pre-BötC with a vibroslicer (Campden Instruments). Slices were stored in artificial CSF (ACSF) at room temperature (i.e., 20°C–23°C) for at least 30 minutes before experiments were started. Subsequently, slices were transferred to the recording chamber and kept submerged by nylon fibers for mechanical stabilization. The chamber was mounted on an upright microscope (Axioscope FS; Zeiss) and perfused continuously with ACSF (20°C–23°C) at a flow rate of 5–10 ml/min. Whole-cell voltage-clamp recordings were obtained with a Multiclamp 700A amplifier (Axon Instruments). Patch electrodes were pulled from borosilicate glass capillaries (Biomedical Instruments) on a horizontal pipette puller (Zeitz-Instrumente) and filled with patch solution containing 125 mM KCl,

1 mM CaCl$_2$, 2 mM MgCl$_2$, 4 mM Na$_2$ATP, 10 mM EGTA, and 10 mM HEPES (pH adjusted to 7.2 with KOH). Patch electrodes had DC impedances ranging 2–6 MΩ.

Generation of plasmids and transfection of cell lines

Generation of expression constructs. Brain tissue from an adult male mouse was explanted and used for total RNA isolation with the OLS RNA kit according to the manufacturer's instructions (OLS). The total RNA was used in 1-step RT-PCR (Invitrogen) using primer pairs for $Glra3$ (forward, 5′-ATGCCTTGGATAAGACTGCTTTC-3′; reverse, 5′-TTAGTCTTGCT-GCTGATGAATGTC-3′) and $Oprm1$ (forward, 5′-ATGGACAGCAGCGCC-GGCCCAGGG-3′; reverse, 5′-TCACCTGCCAAGCTGGCCTTCCC-3′). The cycling program used for RT-PCR was as follows: initial reverse transcription at 55°C for 30 minutes; denaturation at 94°C for 2 minutes; 40 cycles of denaturation at 94°C for 15 seconds, annealing at 57°C for 30 seconds, and elongation at 68°C for 90 seconds; final elongation step at 68°C for 5 minutes. The resulting RT-PCR fragment was purified from the gel and cloned into pTarget expression vector (Promega). Sequencing validated the correct insert sequence. The fluorescently tagged fusion construct $Oprm1$-mCherry was constructed by fusion PCR using pTarget-Oprm1 as a template with the primer pair $Oprm1$-F and $Oprm1$-cherry-R (5′-GTCCTCCTC-GCCCTTGCTCACCATCACTGGATGCTGTACACACCC-3′).

Transfection of cell lines. HEK293 cells (ATCC no. CRL-1573) were maintained at 37°C in a humid atmosphere with 5% CO$_2$ and passaged every second day. For transfection, cells were seeded 24 hours prior to transfection at a density of approximately 500,000 cells in 6-well plates (Nunc). Cells were transfected with 3 μg DNA using 6 μl Lipofectamine (Invitrogen) in 2 ml OptiMEM (Invitrogen) per well and kept under normal culture conditions for 20 hours, after which the medium was replaced with fresh OptiMEM.

RT-PCR

For RT-PCR analysis, the VRG, including the pre-BötC, was dissected from corresponding 300-μm-thick cryostat sections of P30 WT and $Glra3^{-/-}$ mice. PCRs were performed as follows: initial denaturation at 99°C for 5 minutes; 32 cycles of denaturation 95°C 30 seconds, annealing 60°C 30 seconds, extension 72°C 30 seconds; final elongation for 5 minutes at 72°C. The following primer pairs were used for gene amplification: $Glra1$ (forward, 5′-CATTGTATTCTTCAGCCTTGC-3′; reverse, 5′-ACAAGTCAGGCTTC-CAGATG-3′), $Glra2$ (forward, 5′-CAAACCACTTCAGGGAAGC-3′; reverse, 5′-CAAATCCAGGGAATCATCTG-3′), $Glra3$ (exon 7 forward, 5′-GGATCCC-GGGCCTCCTTACC-3′; exon 9/10 reverse, 5′-TCCCTCACCTCATCATCC-GTGTC-3′), $Glra4$ (forward, 5′-TGTTCTCTACAGCATCAGATTG-3′; reverse, 5′-CAGGATGACGATGAGTAGGC-3′), $Glrb$ (forward, 5′-GTACTTGT-GCCCATCTCAGC-3′; reverse, 5′-GTCAGTGCATCTGAGCCTCT-3′), $Slc6a5$ (forward, 5′-CACCACTACCATACCGGAG-3′; reverse, 5′-TCCACACAGACA-CAGGACC-3′), $Slc6a9$ (forward, 5′-AGTCAAGTCTTCAGGGAAAGTG-3′; reverse, 5′-TTGGTGATACTGATAATGACGC-3′), $Gphn$ (forward, 5′-CCAA-GATCCTTCTTTGTTGGGTGGG-3′; reverse, 5′-AGAGAGCATGCCCAGAG-GTGTG-3′), $Hprt1$ (forward, 5′-CGGCAGCGTTTCTGAGCCAT-3′; reverse, 5′-TGAGCACACAGAGGGCCACA-3′).

Measuring reduced PKA-mediated phosphorylation of GlyRα3 upon activation of 5-HTR$_{1A}$

Western blotting. HEK293 cells transfected with expression plasmids coding for GlyRα3 and 5-HTR$_{1A}$ were activated by the addition of 50 μM 8-OH-DPAT (5-HTR$_{1A}$ agonist) in DMEM culture medium for 1 or 10 minutes, while HEK293 cells transfected with expression plasmids coding for GlyRα3 and μOR were activated by 30 nM fentanyl (μOR agonist). For recovery, stimulation media was removed, and cells were incubated for 45 minutes in normal cell culture media. Activation was stopped by fast

aspiration of medium and subsequent washes with TBS (Sigma-Aldrich). Cells were resuspended in TBS by pipetting and pelleted by centrifugation at 1,000 g for 1 minute. TBS was aspirated and replaced by homogenization buffer (20 mM Tris-HCl, pH7.4, and 1 mM EDTA). Cells were then homogenized by 30 strokes in a Dounce homogenizer. Cell lysates were centrifuged at 100 g for 5 minutes at 4°C to remove nuclei. Supernatants were transferred to a fresh tube and centrifuged at 21,000 g for 30 minutes at 4°C. The pellet, containing the membrane fraction, was solubilized in 20 μl Membrane Lysis Buffer (20 mM Tris-HCl, pH7.4; 1 mM EDTA; and 0.6% NP-40) supplemented with 20 μM Na-orthovandate and phosphatase inhibitor cocktail (Sigma-Aldrich) and incubated for 30 minutes at 4°C with occasional mixing. Because NP-40 interferes with SDS-PAGE, samples were dialyzed against homogenization buffer for 4–8 hours at 4°C. To ensure equal loading, the same amount of total protein was applied to all wells, with concentrations determined immediately before each gel run using the Bradford assay. For SDS-PAGE, samples were mixed with 4-fold sample buffer and reducing agent (Invitrogen) containing 20 μM Na-orthovandate and phosphatase inhibitor cocktail and boiled for 10 minutes. Proteins were electrophoretically separated using a 4%–12% Nupage Bis-Tris SDS-PAGE (Invitrogen) and transferred onto a PVDF membrane applying a current of 150 mA for 2.5 hours in a semidry transfer chamber. The efficacy of protein transfer was tested with both Ponceau staining of the membrane and Coomassie blue staining of the remaining protein in the gel. The reactions were blocked with 5% (w/v) BSA in TBS (pH 7.4) containing 0.1% (v/v) Tween 20 (TBS-T) for 60 minutes at room temperature and incubated with primary antibodies at room temperature overnight. All buffers used during dialysis, electrophoresis, blotting, and washing steps were supplemented with 20 μM Na-orthovandate. GlyRα3 phosphorylation was probed with a custom-made monoclonal antibody, mAb764 (1:250 dilution), which selectively recognizes the phosphopeptide NH2-CDEVRESRFSFTA-COOH (RESR consensus sequence shown by underline) containing GlyRα3 serine 346, the sole target for PKA phosphorylation in the GlyRα3 intracellular loop (30). After extensive washing, appropriate secondary HRP-conjugated antibodies (Dianova) were used at 1:500 dilution for 2 hours at room temperature. The color reaction was performed with a chemiluminescence kit (Roth). Corresponding immunoblots for GlyRα3 applying rabbit polyclonal antibodies against GlyRα3 (30) were used as an internal standard for each experiment to verify that all samples contained equal amounts of GlyRα3 protein. Using ELISA, we verified that the mAb had activity versus phospho-GlyRα3, but did not show any significant activity against control peptides for non–phospho-GlyRα3, phospho-GlyRα2 (NH2-CDVTRESRFSFSG-COOH), and phospho-GlyRα4 peptides (NH2-CDIIRESRFYFRG-COOH).

Patch-clamp electrophysiology. HEK293 cells were grown in 10-cm culture dishes (Nunclon) in DMEM supplemented with 10% (v/v) fetal calf serum, 2 mM L-glutamine, 0.45% (w/v) glucose, and 100 U/ml penicillin-G plus 100 μg/ml streptomycin in a 5% CO_2/air atmosphere at 37°C. Cells were harvested and plated onto poly-L-lysine–coated 22-mm coverslips and transfected 4–5 hours later using a modified calcium phosphate precipitation method. A total of 2 μg DNA per coverslip (pcDNA3-hGlyRα3L plus pEGFPN1-5HT1A) was incubated with 20 μl of 340 mM CaCl2 and 24 μl of 2-fold HBS for 30 minutes prior to dropwise addition to the plated cells. After 16 hours, HEK cells were used for electrophysiological recording. Patch electrodes had resistances of 4–5 MΩ and were filled with internal solution containing 120 mM KCl, 1 mM MgCl2, 1 mM CaCl2, 10 mM HEPES, 11 mM EGTA, 30 mM KOH, 2 mM ATP, and 0.5 mM GTP (pH 7.11) with 1M NaOH. The Krebs solution consisted of 140 mM NaCl, 4.7 mM KCl, 1.2 mM MgCl2, 2.5 mM CaCl2, 5 mM HEPES, and 11 mM D-glucose, pH 7.4. An Axopatch 200B amplifier (Axon) was used to record whole-cell currents from single HEK293 cells voltage-clamped at –40 mV.

Cells were visualized with a Nikon Diaphot 300 microscope configured for differential interference contrast to identify cells expressing 5-HTR1A–eGFP using epifluorescence. A U-tube rapidly applied 100 μM glycine (exchange rate, approximately 50–100 ms) at intervals of 1 minute. 5-HT (1 μM) was applied in a 10-second pulse via the U-tube in the presence and absence of the specific 5-HTR1A antagonist, WAY 100635 (2 μM). In experiments using the μ-OR, fentanyl (30 nM) was similarly applied via the U-tube. All currents were filtered by a Bessel filter (5 kHz, –36dB per octave). Data were recorded directly onto a Pentium IV 1.8-GHz computer into Clampex 8.0 via a Digidata 1322A (Axon) sampling at 200-μs intervals.

Applied drugs

The following pharmacological substances were used for physiological experiments: 8-OH-DPAT (5-HTR1A agonist; Tocris), WAY 100635 (5-HTR1A antagonist; Sigma-Aldrich), fentanyl citrate salt (μOR agonist; Sigma-Aldrich), and strychnine hydrochloride (GlyR antagonist; Sigma-Aldrich).

Immunohistochemistry

Transgenic mice expressing eGFP under the control of the neuronal GlyT2 were provided by H.U. Zeilhofer (Institute of Pharmacology and Toxicology, ETH-Zürich, Zürich, Switzerland). GlyT2-eGFP mice (P22–P32) were deeply anesthetized with isoflurane (1-Chloro-2,2,2-trifluoroethyl-difluoromethylether; Abbott) until they were unresponsive to a forepaw pinch. A thoracotomy was performed, and animals were transcardially perfused with 50 ml of 0.9% (w/v) NaCl followed by 200 ml of 4% (w/v) phosphate-buffered PFA at a flow rate of 10 ml/min. The brains were removed, postfixed for 4 hours in 4% (w/v) PFA at 4°C, cryoprotected in 10% (w/v) sucrose for 2 hours, and then stored overnight in 30% (w/v) sucrose plus 0.1 M phosphate buffer at 4°C. A series of 40-μm transverse brainstem sections was cut using a freezing microtome (–25°C; Frigocut). The sections were permeabilized with 0.2% (v/v) Triton X-100 for 45 minutes and then transferred for 1 hour into a solution containing 5% (w/v) BSA in PBS to block nonspecific binding sites. The following primary antibodies were diluted (1–5 μg/ml) in a carrier solution containing 2% (w/v) BSA in PBS and applied for 48–72 hours at 4°C: guinea pig polyclonal antibody against 5-HTR1A (catalog no. AB5406; Millipore; ref. 49), rabbit polyclonal antibody against GlyRα3 (30), rabbit polyclonal antibody against GlyRα1 (catalog no. 146003; Synaptic Systems), guinea pig polyclonal antibody against μOR (catalog no. GP10106; Neuromics; ref. 50), guinea pig polyclonal antibody against NK-1R (catalog no. AB15810; Chemicon), and mouse monoclonal antibody against NeuN (catalog no. MAB377; Millipore). After incubation, sections were rinsed 3 times in PBS and subsequently incubated for 4 hours in the dark with species-specific secondary antibodies conjugated with fluorochromes Cy2, Cy3, or Cy5 (Dianova). The secondary antibodies were diluted 1:500 in 2% (w/v) BSA in PBS. Following the last incubation, the sections were rinsed 3 times in PBS, mounted onto microscope slides, and finally coverslipped with fluorescent mounting medium (DAKO). Analysis of neuronal immunofluorescence was performed with a confocal laser-scanning microscope (LSM 510 Meta; Zeiss). For data acquisition and analysis of the confocal images, we used LSM 510 Meta software (Zeiss). Subsequent imaging procedures (cell counting) were performed using ImageJ (http://rsb.info.nih.gov/ij/). The pre-BötC was identified by anatomical landmarks such as the principal nucleus of the inferior olive and the nucleus ambiguus and by corresponding sections stained for a known pre-BötC marker, the substance P–reactive NK-1R. Anatomical structures were described as previously published (51).

Statistics

Data from pharmacological experiments of perfused brainstem preparations were statistically analyzed using repeated-measures ANOVA with

Bonferroni multiple-comparison test and were performed using Graph-Pad Prism (version 5.0c for Mac OSX; GraphPad Software). Differences were considered statistically significant at the $P < 0.05$ level. To quantify the PN activity from electrophysiological recordings, a representative measurement of 1-minute duration before and after each drug application (10–15 minute interval) was integrated with LabChart 7 software (ADInstruments). The results, given as integrated mPNA (units of V•s), were normalized to the control, defined as 1.0 (n, no. animals). Data are presented as the mean ± SEM of AU. The differences in the time durations of inspiration, post-inspiration, and expiration analyzed for each burst per representative 1-minute period of the 3 phases of the respiratory cycle of WT and $Glra3^{-/-}$ mice derived from integrated recordings of PN activity (n, no. animals) were given as means ± SEM. Significance was statistically verified by the unpaired t test for each phase. In addition, the CV was used to illustrate the relative variability (SD divided by mean). Data are presented as mean CV ± SEM. Electrophysiological data of I_{Gly} recorded from HEK293 cells were normalized to I_{Gly} measured at 0 minutes, which was set to 1.0 (n, no. cells). Data of cell experiments were statistically analyzed with repeated-measures ANOVA followed by Bonferroni post-hoc test. Immunoblot data were normalized to non-stimulated cell sample, which was set to 1.0 after densitometric measurement of corresponding signals (n, no. experiments), statistically analyzed with 1-way ANOVA followed by Bonferroni post-hoc test, and presented as mean ± SEM of AU. Immunohistochemical data (cell counting) are presented as mean ± SEM of labeled cells within the bilateral pre-BötC region per section.

Address correspondence to: Diethelm W. Richter, Department of Neuro- and Sensory Physiology, University Medicine Göttingen, Germany. Phone: 49551.39.5911; Fax: 49551.39.6031; E-mail: d.richter@gwdg.de.

1. Smith JC, Ellenberger HH, Ballanyi K, Richter DW, Feldman JL. Pre-Bötzinger complex: a brainstem region that may generate respiratory rhythm in mammals. *Science*. 1991;254(5032):726–729.
2. Smith JC, Abdala AP, Koizumi H, Rybak IA, Paton JF. Spatial and functional architecture of the mammalian brain stem respiratory network: a hierarchy of three oscillatory mechanisms. *J Neurophysiol*. 2007;98(6):3370–3387.
3. Dick TE, Bellingham MC, Richter DW. Pontine respiratory neurons in anesthetized cats. *Brain Res*. 1994;636(2):259–269.
4. Mörschel M, Dutschmann M. Pontine respiratory activity involved in inspiratory/expiratory phase transition. *Philos Trans R Soc Lond B Biol Sci*. 2009; 364(1529):2517–2226.
5. Richter DW. Generation and maintenance of the respiratory rhythm. *J Exp Biol*. 1982;100:93–107.
6. Smith JC, Butera RJ, Koshiya N, Del Negro C, Wilson CG, Johnson SM. Respiratory rhythm generation in neonatal and adult mammals: the hybrid pacemaker-network model. *Respir Physiol*. 2000; 122(2–3):131–147.
7. Richter DW, Spyer KM. Studying rhythmogenesis of breathing: comparison of in vivo and in vitro models. *Trends Neurosci*. 2001;24(8):464–472.
8. Rybak IA, et al. Modeling the ponto-medullary respiratory network. *Respir Physiol Neurobiol*. 2004; 143(2–3):307–319.
9. Ogilvie MD, Gottschalk A, Anders K, Richter DW, Pack AI. A network model of respiratory rhythmogenesis. *Am J Physiol*. 1992;263(4 pt 2):R962–R975.
10. Richter DW. Neural regulation of respiration: rhythmogenesis and afferent control. In: Greger R, Windhorst U, eds. *Comprehensive Human Physiology*. 1st ed. Berlin, Germany: Springer-Verlag; 1996:2079–2095.
11. Schmid K, Bohmer G, Gebauer K. Glycine receptor-mediated fast synaptic inhibition in the brainstem respiratory system. *Respir Physiol*. 1991;84(3):351–361.
12. Pierrefiche O, Schwarzacher SW, Bischoff AM, Richter DW. Blockade of synaptic inhibition within the pre-Botzinger complex in the cat suppresses respiratory rhythm generation in vivo. *J Physiol*. 1998;509(pt 1):245–254.
13. Busselberg D, Bischoff AM, Becker K, Becker CM, Richter DW. The respiratory rhythm in mutant oscillator mice. *Neurosci Lett*. 2001;316(2):99–102.
14. Wilken B, et al. Treatment of apneustic respiratory disturbance with a serotonin-receptor agonist. *J Pediatr*. 1997;130(1):89–94.
15. Richter DW, Manzke T, Wilken B, Ponimaskin E. Serotonin receptors: guardians of stable breathing. *Trends Mol Med*. 2003;9(12):542–548.
16. El-Khatib MF, Kiwan RA, Jamaleddine GW. Buspirone treatment for apneustic breathing in brain stem infarct. *Respir Care*. 2003;48(10):956–958.
17. Stettner GM, Huppke P, Brendel C, Richter DW, Gärtner J, Dutschmann M. Breathing dysfunctions associated with impaired control of postinspiratory activity in Mecp2-/y knockout mice. *J Physiol*. 2007;579(pt 3):863–876.
18. Richter DW, Bischoff A, Anders K, Bellingham M, Windhorst U. Response of the medullary respiratory network of the cat to hypoxia. *J Physiol*. 1991; 443:231–256.
19. Stewart J, Howard RS, Rudd AG, Woolf C, Russell RW. Apneustic breathing provoked by limbic influences. *Postgrad Med J*. 1996;72(851):559–561.
20. Harrison NL, Kugler JL, Jones MV, Greenblatt EP, Pritchett DB. Positive modulation of human γ-aminobutyric acid type A and glycine receptors by the inhalation anesthetic isoflurane. *Mol Pharmacol*. 1993;44(3):628–632.
21. Manzke T, et al. Serotonin targets inhibitory neurones to induce complex modulation of network functions. *Philos Trans R Soc Lond B Biol Sci*. 2009; 364(1529):2589–2602.
22. Celentano JJ, Gibbs TT, Farb DH. Ethanol potentiates GABA- and glycine-induced chloride currents in chick spinal cord neurons. *Brain Res*. 1988; 455(2):377–380.
23. Richter DW, et al. Intracellular signal pathways controlling respiratory neurons. *Respir Physiol*. 1997; 110(2–3):113–123.
24. Hoyer D, Hannon JP, Martin GR. Molecular, pharmacological and functional diversity of 5-HT receptors. *Pharmacol Biochem Behav*. 2002;71(4):533–554.
25. Lalley PM, Pierrefiche O, Bischoff AM, Richter DW. cAMP-dependent protein kinase modulates expiratory neurons in vivo. *J Neurophysiol*. 1997; 77(3):1119–1131.
26. Zeilhofer HU, et al. Glycinergic neurons expressing enhanced green fluorescent protein in bacterial artificial chromosome transgenic mice. *J Comp Neurol*. 2005;482(2):123–141.
27. Gray PA, Rekling JC, Bocchiaro CM, Feldman JL. Modulation of respiratory frequency by peptidergic input to rhythmogenic neurons in the preBotzinger complex. *Science*. 1999;286(5444):1566–1568.
28. Guyenet PG, Wang H. Pre-Bötzinger neurons with preinspiratory discharges "in vivo" express NK1 receptors in the rat. *J Neurophysiol*. 2001;86(1):438–446.
29. Winter SM, Fresemann J, Schnell C, Oku Y, Hirrlinger J, Hulsmann S. Glycinergic interneurons are functionally integrated into the inspiratory network of mouse medullary slices. *Pflugers Arch*. 2009; 458(3):459–469.
30. Harvey RJ, et al. GlyR α3: an essential target for spinal PGE$_2$-mediated inflammatory pain sensitization. *Science*. 2004;304(5672):884–887.
31. Connelly CA, Ellenberger HH, Feldman JL. Are there serotonergic projections from raphe and retrotrapezoid nuclei to the ventral respiratory group in the rat? *Neurosci Lett*. 1989;105(1–2):34–40.
32. Richter DW, Schmidt-Garcon P, Pierrefiche O, Bischoff AM, Lalley PM. Neurotransmitters and neuromodulators controlling the hypoxic respiratory response in anaesthetized cats. *J Physiol*. 1999;514(pt 2):567–578.
33. Heindl C, Brune K, Renner B. Kinetics and functional characterization of the glycine receptor α2 and α3 subunit. *Neurosci Lett*. 2007;429(1):59–63.
34. Paton JF. A working heart-brainstem preparation of the mouse. *J Neurosci Methods*. 1996;65(1):63–68.
35. Ballanyi K, Lalley PM, Hoch B, Richter DW. cAMP-dependent reversal of opioid- and prostaglandin-mediated depression of the isolated respiratory network in newborn rats. *J Physiol*. 1997;504(pt 1):127–134.
36. Guenther U, et al. The counteraction of opioid-induced ventilatory depression by the serotonin 1A-agonist 8-OH-DPAT does not antagonize antinociception in rats in situ and in vivo. *Anesth Analg*. 2009;108(4):1169–1176.
37. Sahibzada N, Ferreira M, Wasserman AM, Taveira-DaSilva AM, Gillis RA. Reversal of morphine-induced apnea in the anesthetized rat by drugs that activate 5-hydroxytryptamine$_{1A}$ receptors. *J Pharmacol Exp Ther*. 2000;292(2):704–713.
38. Ezure K, Tanaka I, Kondo M. Glycine is used as a transmitter by decrementing expiratory neurons of the ventrolateral medulla in the rat. *J Neurosci*. 2003;23(26):8941–8948.
39. Klages S, Bellingham MC, Richter DW. Late expiratory inhibition of stage 2 expiratory neurons in the cat - a correlate of expiratory termination. *J Neurophysiol*. 1993;70(4):1307–1315.
40. Gomeza J, et al. Deletion of the mouse glycine transporter 2 results in a hyperekplexia phenotype and postnatal lethality. *Neuron*. 2003;40(4):797–806.
41. Markstahler U, Kremer E, Kimmina S, Becker K, Richter DW. Effects of functional knock-out of alpha 1 glycine-receptors on breathing movements

in oscillator mice. *Respir Physiol Neurobiol*. 2002; 130(1):33–42.

42. Mason P. Physiological identification of ponto-medullary serotonergic neurons in the rat. *J Neurophysiol*. 1997;77(3):1087–1098.

43. Renner U, et al. Localization of the mouse 5-hydroxytryptamine(1A) receptor in lipid microdomains depends on its palmitoylation and is involved in receptor-mediated signaling. *Mol Pharmacol*. 2007; 72(3):502–513.

44. Zhang L, Zhao H, Qiu Y, Loh HH, Law PY. *Src* phosphorylation of micro-receptor is responsible for the receptor switching from an inhibitory to a stimulatory signal. *J Biol Chem*. 2009;284(4):1990–2000.

45. Murthy KS, Makhlouf GH. Opioid mu, delta, and kappa receptor-induced activation of phospholipase C-beta 3 and inhibition of adenylyl cyclase is mediated by Gi2 and G(o) in smooth muscle. *Mol Pharmacol*. 1996;50(4):870–877.

46. Busselberg D, Bischoff AM, Paton JF, Richter DW. Reorganisation of respiratory network activity after loss of glycinergic inhibition. *Pflugers Arch*. 2001; 441(4):444–449.

47. Busselberg D, Bischoff AM, Richter DW. A combined blockade of glycine and calcium-dependent potassium channels abolishes the respiratory rhythm. *NeuroScience*. 2003;122(3):831–841.

48. Haverkamp S, Müller U, Harvey K, Harvey RJ, Betz H, Wässle H. Diversity of glycine receptors in the mouse retina: localization of the alpha3 subunit. *J Comp Neurol*. 2003;465(4):524–539.

49. Kirby LG, Pernar L, Valentino RJ, Beck SG. Distinguishing characteristics of serotonin and non-serotonin-containing cells in the dorsal raphe nucleus: electrophysiological and immunohistochemical studies. *NeuroScience*. 2003;116(3):669–683.

50. Arvidsson U, et al. Distribution and targeting of a mu-opioid receptor (MOR1) in brain and spinal cord. *J Neurosci*. 1995;15(5 pt 1):3328–3341.

51. Paxinos G, Franklin KBJ. *The Mouse Brain in Stereotaxic Coordinates*. San Diego, California, USA: Academic Press; 2001.